

Effects of Liquid Fuel Mass Fraction and Droplet Size on Droplet Group Combustion Behavior

Mariko Nakamura¹, Fumiteru Akamatsu¹, Ryoichi Kurose², and Masashi Katsuki¹

¹Department of Mechanical Engineering, Osaka University, 2-1 Yamadaoka, Suita, Osaka 565-0871, JAPAN

²Energy Engineering Research Laboratory, Central Research Institute of Electric Power Industry (CRIEPI), 2-6-1 Nagasaka, Yokosuka, Kanagawa 240-0196, JAPAN

Corresponding author, Fumiteru Akamatsu: akamatsu@mech.eng.osaka-u.ac.jp

Introduction

Spray combustion is used in numerous engineering applications such as energy conversion and prime movers. It is, therefore, necessary to precisely predict combustion behaviors of spray in designing the devices. However, it is one of the most complex fields where dispersion of fuel droplets, their evaporation, chemical reactions of fuel vapor with oxidizer and so on take place simultaneously interacting each other. Therefore, the underlying physics governing these processes has not been well understood.

To verify the presence of the droplet group combustion¹ in actual spray flames, Akamatsu and co-workers^{2,4} have applied the advanced laser-based diagnostics with high temporal and spatial resolutions to spray flames stabilized in turbulent jet and laminar counterflows. They observed the droplet group combustion in such flames and showed that the behavior of the droplet group combustion differs depending on the supplied condition and characteristics of liquid fuel spray. However, the detailed mechanism has not been clarified yet, because it is impossible at present to measure all the physical quantities in spray flames simultaneously. Accordingly, we have conducted two-dimensional direct numerical simulations (DNS) for spray flames stabilized in a laminar counterflow used in the experiment⁵⁻⁷.

In this paper, the effects of liquid fuel mass fraction in two-phase flow and droplet size on the spray combustion behavior are studied by two-dimensional DNS of spray flames formed in a laminar counterflow, and the droplet group combustion theory¹ is discussed based on the calculated spray characteristics. Spray flames stabilized in counterflow field have been accepted as a useful tool in

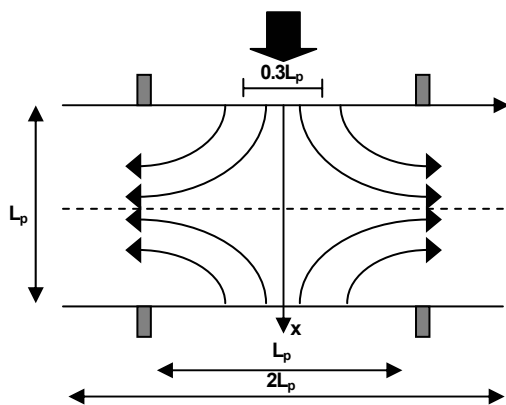


Fig. 1 Computational domain for DNS

investigating their detailed structure⁸⁻¹⁰, and for the numerical calculations of the counterflow spray flames, a similarity solution⁹, in which the flow-field is treated as one dimensional, is often employed. However, strictly speaking, this method can be applied only to the special case where monodisperse small-sized spray of highly volatile liquid fuel is used and almost all droplets prevaporize before entering the reaction zone. Consequently, our numerical simulations are conducted without using a similarity solution.

Numerical Method

The governing equations considered for the gaseous phase were mass, momentum, energy, and species mass conservation⁶. All the fuel droplets were tracked individually in a Lagrangian manner. Concerning the vaporization of droplets, a non-equilibrium Langmuir-Knudsen evaporation model was chosen¹¹. For the droplet motion, we adopted the drag coefficient of a droplet proposed by Kurose et al.¹².

The computational domain used in this study is shown in Fig. 1. The dimensions of the computational domain normalized by the diameter of burner ports, L_p , are 1 and 2 in the x and y directions, respectively. In this paper, the length scales x and y normalized by L_p are shown as x^* and y^* , respectively. The origin of the calculation domain is located at the center of the upper burner port. From the upper port of $-0.5 \leq y^* \leq 0.5$, atmospheric air ($T = 300$ K, $P = 0.1013$ MPa, and oxygen mass fraction $Y_{O_2} = 0.2357$) is issued. From the lower port, premixture of atmospheric air and n-decane ($C_{10}H_{22}$) vapor (equivalence ratio, $\phi = 0.6$) is issued in the region of $-0.15 \leq y^* \leq 0.15$, and atmospheric air is issued in the region of $-0.5 \leq y^* \leq -0.15$ and $0.15 \leq y^* \leq 0.5$. The n-decane ($C_{10}H_{22}$) spray is injected from the upper port in the range of $-0.15 \leq y^* \leq 0.15$. The fluid velocities issued from the upper and lower ports are the same. The Reynolds number based on the burner port diameter, L_p ($= 0.02$ m), the fluid velocity, u_0 ($= 0.4$ m/s), and cold air properties is 500. The stretch ratio of the laminar counterflow is 40 1/s.

The governing equations for the gaseous phase are discretized and solved by a finite volume method using SIMPLE algorithm¹³. The calculation domain ($0 \leq x^* \leq 1$, $-1 \leq y^* \leq 1$) is divided into 200×400 equally spaced computational cells in x and y directions, respectively. The spatial integration is approximated by a fourth-order central difference scheme and the time integration is performed via a fully implicit method. Dispersed droplets are randomly injected on the upper port of $-0.15 \leq y^* \leq 0.15$ and tracked in a Lagrangian manner. The equations of droplet behavior are integrated using a second-order Adams-Bashforth scheme. Mass, heat, and momentum interactions between gaseous and disperse phases are evaluated on the basis of the control volume of the gaseous phase calculation¹⁴. Interaction terms between phases during a calculation time step are considered at the final droplet location of the time step.

For the combustion reaction, one-step global reaction model of n-decane¹⁵ is adopted. Gaseous species considered in the calculations are O_2 , N_2 , CO_2 , H_2O , and $C_{10}H_{22}$, and their transport properties and thermodynamic data are obtained from CHEMKIN^{16,17}. To consider the temperature dependence of properties of liquid n-decane, the density, the heat conductivity, and the specific heat of liquid n-decane

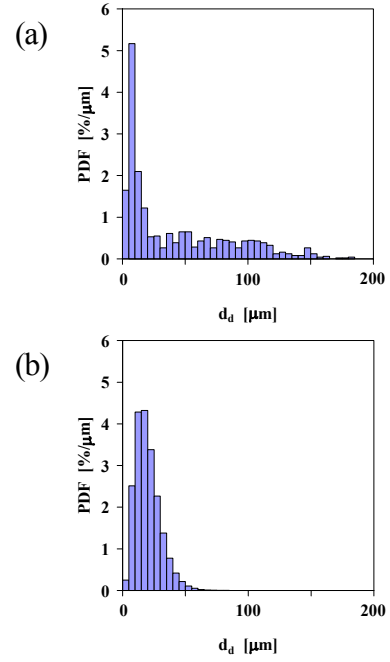


Fig.2 Initial droplet size distributions: (a) SMD = 106.7 μm ; (b) SMD = 30 μm

are obtained from Gunn-Yamada equation, Sato-Riedel equation, and Sterning-Brown equation, respectively¹⁸.

Firstly, the computation was conducted for the spray equivalence ratio of $\phi_l = 0.42$, which was the same value as the time-averaged equivalence ratio of spray in the experiment, with the initial droplet size distribution of Fig. 2(a). Fig. 2(a) was obtained from the PDA measurement, and Fig. 2(b) was assumed using Nukiyama-Tanazawa distribution function. Secondly, the computations were performed for three different spray equivalence ratios of $\phi_l = 0.21, 0.63,$ and 1.26 with different initial droplet size distribution in Fig. 2.

Results and Discussion

Fig. 3 shows the comparisons of axial profiles of droplet mean axial velocity, \bar{u}_d / u_0 , arithmetic mean diameter, AMD , and Sauter mean diameter, SMD , between experiment and computation for $\phi_l = 0.42$. The computed results agree qualitatively with the experimental ones. The droplet mean velocity, \bar{u}_d / u_0 , initially increases but subsequently decreases. The droplet mean diameters, AMD and SMD , increase as x^* increases. The increases of AMD and SMD are due to the evaporation and the lower inertia of the smaller droplets, which allows most of them to move away from the x axis, following the outward flow. Quantitatively, computed \bar{u}_d / u_0 , AMD , and SMD are smaller than the experimental values. This is because the larger droplets, which are not included in Fig. 2 (a), are often generated in the experiments. Although the mass fraction of such larger droplets is approximately 1%, the mean droplet diameter and axial velocity are increased due to their larger inertias.

Axial profiles of mean gaseous temperature, \bar{T} , for $\phi_l = 0.21, 0.63$ and 1.26 for two types of droplet size distribution are shown in Fig. 4. In general, as the spray equivalence ratio, ϕ_l , increases, the high temperature region expands, which seems reasonable because the calorific value of added spray increases with increasing ϕ_l . However, in the case of the larger droplet size, in the upper part of the high temperature region of $0.3 \leq x^* \leq 0.5$, the value of temperature tends to decrease for high spray equivalence ratios of $\phi_l = 1.26$ by comparing with the case of $\phi_l = 0.63$. For the smaller droplet size, the high temperature region moves to the upstream side and the peak value monotonously

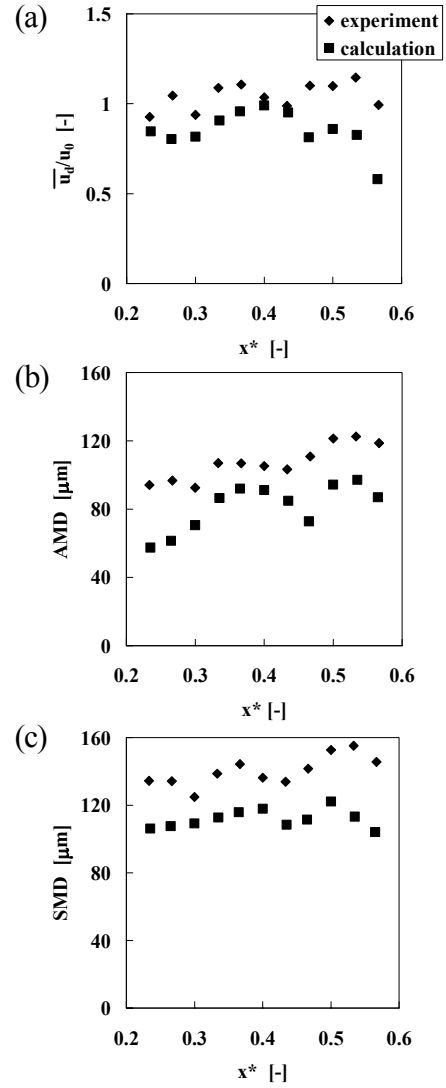


Fig.3 Comparisons of axial profiles of (a) mean axial velocity; (b) arithmetic mean diameter; (c) Sauter mean diameter for $\phi_l = 0.42$

increases with increasing ϕ_l .

To investigate the spray combustion behavior in detail and understand the reason why the gaseous temperature decreases for high spray equivalence ratios in the region of $0.3 \leq x^* \leq 0.5$, the instantaneous distributions of gaseous temperature, T , combustion reaction rate, R_F , and gaseous equivalence ratio, ϕ for $\phi_l = 1.26$ are illustrated in Fig. 5. Only the central region of $-0.15 \leq y^* \leq 0.15$ is shown. Here, droplet locations are shown only for the larger droplet size

distribution. The high combustion reaction rate around $x^* = 0.75$ in the figure of R_F is due to the gaseous flame of premixture supplied from the lower port. The global spray combustion field for larger droplet size exhibits two different combustion zones judging from the distributions of R_F and ϕ . First, for larger droplet size, the high R_F zone appears around the front surface of the high \bar{T} region at $x^* = 0.25$. Although the droplets continuously evaporate even in the upstream portion of this zone (see the figure

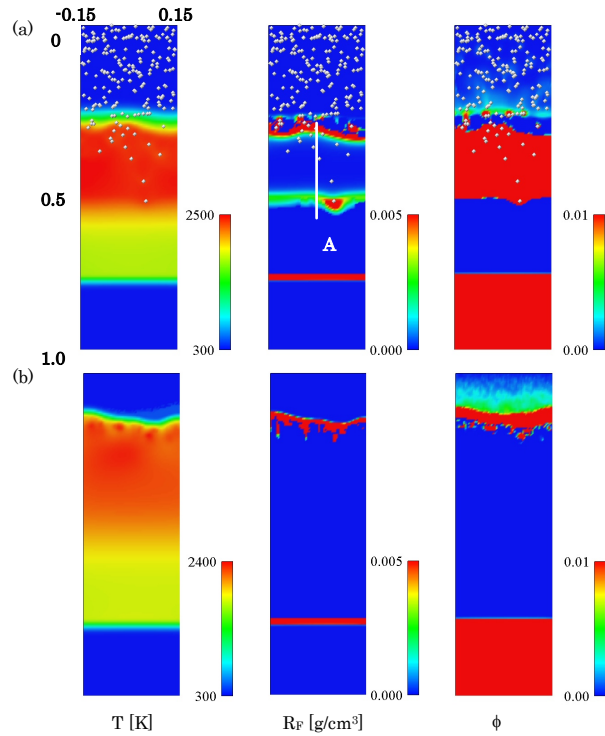


Fig. 5 Instantaneous distributions of gaseous temperature, T , combustion reaction rate, R_F and gaseous equivalence ratio, ϕ . (a) SMD = 106.7 μm ; (b) SMD = 30 μm

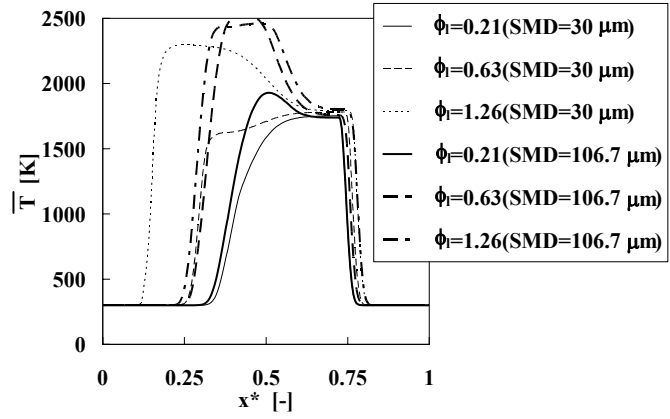


Fig.4 Axial profiles of mean gaseous temperature

of ϕ), the combustion does not occur until the fuel vapor reaches this zone. We can consider that a 'premixed-like combustion' takes place in this zone, since the fuel vapor mixes with air before reactions start. Subsequently, in the downstream portion of $0.25 \leq x^* \leq 0.5$, there appears a 'diffusion-like combustion' zone, where the continuous evaporation and combustion of the remaining droplets take place passing through the 'premixed-like combustion' zone at the same time.

Furthermore, this 'diffusion-like combustion' is apparently divided into two different combustion types. The remaining droplets in the high temperature region evaporate and burn individually in the upper region ($0.25 \leq x^* \leq 0.3$), and burn as clusters including some droplets in the lower region ($0.3 \leq x^* \leq 0.5$). The difference in the combustion type can be understood by

Figure 6, which shows the instantaneous axial profiles of gaseous temperature, T , mass fraction of O_2 and $C_{10}H_{22}$, Y_{O_2} and $Y_{C_{10}H_{22}}$, and combustion reaction rate, R_F , in Figure 5(a). The oxygen is abundant in the upper region of $0.25 \leq x^* \leq 0.3$, but almost zero in the lower region of $0.3 \leq x^* \leq 0.5$. Therefore, the fuel vapor generated in the high temperature region reacts immediately with the oxygen and is consumed in the former condition, whereas it is not consumed in the latter condition. Consequently, the high fuel vapor lumps containing some droplets burn from the outer surface where the oxygen is abundant.

The phenomenon, in which the droplets burn as a cluster described above, is called as '*droplet group combustion*'. The high fuel vapor lumps containing some droplets shown Figure 5(a) would correspond to *external combustion*. Here, the corresponding calculated G number¹ is 5.41, provided that Lewis number = 1.0 and $Re_{sl} = 0$, and the total number of droplets contained in the cluster and the mean separation distance between droplet centers are estimated for the mixture of unburned fuel droplets and air.

For the smaller droplet size, because the small droplets complete evaporation and vanish before entering into the high temperature region, the combustion is rounded off only in the '*premixed-like combustion*'. Consequently, the *droplet group combustion* does not appear. The decrease of the gaseous temperature for high spray equivalence ratio of $\phi_l = 1.26$ in the high region of $0.3 \leq x^* \leq 0.5$, as shown before, is considered to be related to this group combustion behavior. It is verified that the droplet group combustion tends to reduce the gaseous temperature and this is caused mainly by the suppression of combustion reaction due to the lack of oxygen.

The actual spray flames cannot eliminate the influences of droplet size distribution, and therefore spray combustion is characterized by the flame structure in which '*diffusion-like combustion*' formed by larger droplets coexists with '*premixed-like combustion*' of prevaporised fuel in inter-space of droplets. However, the enhancement of atomization and evaporation of liquid fuel would prevent local temperature drop or soot formation resulting from the '*diffusion-like combustion*' of droplet clusters.

Conclusions

Two-dimensional DNS was applied to spray flames formed in a laminar counterflow, and the detailed flame structure was examined. With increasing the droplet mass flow rate, two types of spray combustions, i.e. '*premixed-like combustion*' and '*diffusion-like combustion*', appeared in front of and inside of the high temperature region, respectively. The *droplet group combustion* behavior was observed in the '*diffusion-like combustion*' region. It was also verified that the droplet group combustion

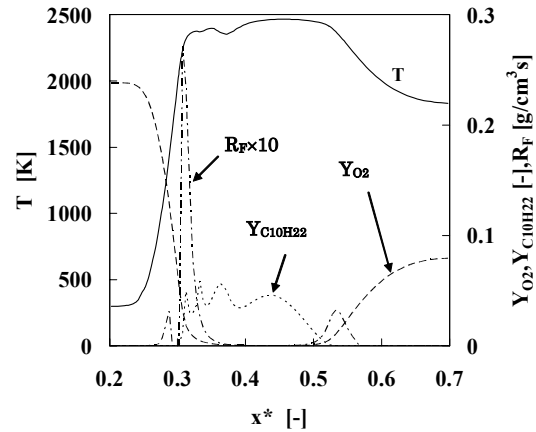


Fig. 6 Instantaneous profiles of gaseous temperature, mass fraction of O_2 and $C_{10}H_{22}$, and combustion reaction rate on the A section in Fig. 5(a)

tends to decrease the gaseous temperature resulting mainly from the depression of combustion reaction due to the lack of oxygen. It was shown that the 'diffusion-like combustion' does not appear for small droplets spray, because the droplets complete their evaporation before entering into the high gaseous temperature region.

References

- ¹ H. H. Chiu, H. Y. Kim and E. J. Croke 1982 "International group combustion of liquid droplets," Proc. Combust. Inst. 19, 971-980.
- ² F. Akamatsu, Y. Mizutani, M. Katsuki, S. Tsushima and Y. D. Cho 1996 "Measurement of the local group combustion number of droplet clusters in a premixed spray stream," Proc. Combust. Inst. 26, 1723-1729.
- ³ S. Tsushima, H. Saitoh, F. Akamatsu and M. Katsuki 1998 "Observation of combustion characteristics of droplet clusters in a premixed-spray flame by simultaneous monitoring of planar spray images and local chemiluminescence," Proc. Combust. Inst. 27, 1967-1974.
- ⁴ T. Wakabayashi, Y. Mizutani, M. Katsuki and F. Akamatsu 1998 "Observation of the structure of a spray flame in 2-D counterflow burner," 36th AIAA Aerospace Sciences Meeting, Paper No. 98-0720.
- ⁵ F. Akamatsu, H. Saitoh and M. Katsuki 2000 "Numerical simulation of spray flat flames stabilized in a laminar counterflow," Proc. 8th Conference on liquid atomization and spray systems, ICLASS-2000, 25-32.
- ⁶ M. Nakamura, F. Akamatsu, R. Kurose and M. Katsuki "Combustion mechanism of liquid fuel spray entering gaseous flame front," Journal of the Japan Society of Mechanical Engineers, in Japanese, accepted.
- ⁷ R. Kurose, O. Desjardins, M. Nakamura, F. Akamatsu and H. Pitsch 2004 "Numerical simulation of spray flames," Annual Research Brief-2004, Center for Turbulence Research, NASA Ames/Stanford University, 269-280.
- ⁸ J. B. Greenberg, D. Albagli, and Y. Tambour 1986 "An opposed jet quasi-monodisperse spray diffusion flame," Combust. Sci. Tech. 50, 255-270.
- ⁹ G. Continillo and W. A. Sirignano 1990 "Counterflow Spray Combustion Modeling," Combust. Flame 81, 325-340.
- ¹⁰ E. Gutheil and W. A. Sirignano 1998 "Counterflow spray combustion modeling with detailed transport and detailed chemistry," Combust. Flame 113, 92-105.
- ¹¹ R. S. Miller and J. Bellan 1999 "Direct numerical simulation of a confined three-dimensional gas mixing layer with one evaporating hydrocarbon-droplet-laden stream." J. Fluid Mech. 384, 293-338.
- ¹² R. Kurose, H. Makino, S. Komori, M. Nakamura, F. Akamatsu and M. Katsuki 2003 "Effects of outflow from the surface of a sphere on drag, shear lift, and scalar diffusion," Phys. Fluids 15, 2338-2351.
- ¹³ S. V. Patankar 1980 "Numerical Heat Transfer and Fluid Flow," McGraw-Hill.
- ¹⁴ C. T. Crowe, M. P. Sharma and D. E. Stock 1977 "The particle-source-in cell (PSI-CELL) model for gas-droplet flows," ASME J. of Fluids Eng. 99, 325-332.
- ¹⁵ C. K. Westbrook and F. L. Dryer 1984 "Chemical kinetic modeling of hydrocarbon combustion," Prog. Energy Combust. Sci., 10, 1-57.
- ¹⁶ R. J. Kee, G. Dixon-Lewis, J. Warnatz, M. E. Coltrin and J. A. Miller 1986 "A fortran computer code package for the evaluation of gas-phase multicomponent transport properties," SANDIA Report,

SAND86-8246.

¹⁷R. J. Kee, F. M. Rupley and J. A. Miller 1989 “Chemkin-II: A fortran chemical kinetics package for the analysis of gas phase chemical kinetics”, SANDIA Report, SAND89-8009B.

¹⁸R. C. Reid, J. M. Prausnitz and T. K. Sherwood 1977 “The Properties of Gases and Liquids, third edition,” McGraw-Hill, New York.